

# Studies on structural transformation and magnetic properties in $\text{Sm}_2\text{Co}_{17}$ type alloys

R. GOPALAN, K. MURALEEDHARAN, T. S. R. K. SASTRY, A. K. SINGH,  
V. JOSHI, D. V. SRIDHARA RAO, V. CHANDRASEKARAN  
*Defence Metallurgical Research Laboratory, Hyderabad-500 058, India*  
E-mail: gopalan@dmrl.ernet.in

Structural transformations and microstructural characterisation of  $\text{Sm}_2\text{Co}_{17}$  alloys containing Fe, Cu and Zr at different stages of thermal processing have been investigated by X-ray diffraction, optical, scanning electron and transmission electron microscopes. Solution treated samples consist of a mixture of hexagonal  $\text{TbCu}_7$  (1:7 H) and rhombohedral  $\text{Th}_2\text{Zn}_{17}$  (2:17 R) structure types of 2:17 phase. After isothermal aging,  $\text{TbCu}_7 + \text{Th}_2\text{Zn}_{17}$  structures transform into  $\text{Th}_2\text{Zn}_{17}$  type structure with precipitation of Cu-rich hexagonal  $\text{SmCo}_5$  (1:5 H) and Zr-rich platelet phases. In addition to the main phases, a soft magnetic phase of composition  $\text{Zr}_6(\text{FeCo})_{23}$  is formed in alloys containing higher Zr composition. Isothermal aging studies reveal that magnetic properties show a peak value when aged at 1108–1123 K for 10 h. TEM studies show cellular precipitate structure with cell interiors having 2:17 R structure, while the fully coherent cell boundaries have the 1:5 H structure. Zr-rich platelets which run across many cells and cell boundaries were found to have 1:7 H structure. © 2001 Kluwer Academic Publishers

## 1. Introduction

$\text{Sm}_2\text{Co}_{17}$  (2:17 type) alloys containing Fe, Cu and Zr are technologically important permanent magnet materials for high temperature applications by virtue of their excellent combination of energy product and thermal stability [1, 2]. The hard magnetic properties in these alloys are attributed to the development of a fine scale cellular precipitate microstructure achieved through a multi-stage heat-treatment procedure, *viz.* sintering and solution treatment (1433 K–1483 K) and isothermal aging (1073–1173 K) followed by slow cooling to 673 K. The fine scale microstructure consists of rhombohedral  $\text{Sm}_2(\text{CoFe})_{17}$  [2:17 R] phase as cells surrounded by hexagonal  $\text{Sm}(\text{CoCu})_5$  [1:5 H] boundary phase with Zr-rich platelet phase running across cells and cell boundaries [3–6]. The cell boundary and the platelet phases act as pinning centres for domain walls and the material exhibits a good combination of permanent magnet characteristics. The exact mechanism by which cellular precipitation occurs and of the structure dependent coercivity mechanism are still topics of current research. It has been reported that formation of the  $\text{TbCu}_7$  (1:7 H) structure during the solution treatment stage is essential for the development of large intrinsic coercivity (iHc) in 2:17 type magnets [7–10]. This is because, the anisotropy of the 1:7 H structure is greater than that of  $\text{Th}_2\text{Zn}_{17}$  (2:17 R) type structure. In addition to the formation of the 1:7 H structure, the time–temperature parameters of isothermal aging and the volume fraction of the secondary phase (1:5 type) also play a major role in influencing the fine scale microstructure and the mag-

netic properties of the 2:17 type magnets [11]. Hence it is of scientific interest and technological importance to study the phase formation in 2:17 SmCo system at various stages of heat-treatment and its dependence on magnetic properties.

An attempt has been made in the present study to investigate the structural transformations at various stages of thermal processing of 2:17 type SmCo alloys containing Co-(9–12)Sm-(18–22)Fe-(4–5)Cu-(3–4)Zr (all compositions in at%). A systematic study on the effect of isothermal aging time and temperature on magnetic properties has also been carried out to establish a relationship between the phase formation and the properties.

## 2. Experimental

Three alloys (A, B and C) with nominal compositions as given in Table I were prepared from high purity constituent elements by melting under argon atmosphere. The ingots were crushed and milled down to about 5–10  $\mu\text{m}$ . A magnetic field of about 2000 kA/m was used to align the powders and cylindrical samples were die-pressed. The green compacts, after sintering and solution treatment, were subjected to isothermal aging between 1073 K to 1148 K for 10 h and slow cooled to 673 K at the rate of 30 K/h.

X-ray diffraction (XRD) patterns were obtained using a Philip X-ray powder diffractometer, PW3020 with  $\text{Cu K}\alpha$  radiation. Microstructural studies were carried out using optical, scanning electron (Leo 440i SEM) and transmission electron microscopes (Philip EM 430T operating at 200 kV) with energy dispersive

TABLE I Nominal compositions of the alloys

Alloy	Composition (at%)				
	Sm	Co	Fe	Cu	Zr
A	11.5	60.0	21.0	4.5	3.0
B	10.5	63.0	22.0	4.0	3.5
C	9.5	64.5	18.0	4.0	4.0

X-ray analysis (EDS). Specimens for TEM samples were prepared by dimpling and ion milling. Magnetic measurements were performed on disk samples using auto hysteresis graph (Walker Scientific Inc.).

### 3. Results and discussion

#### 3.1. Phase diagram and crystal structure types

In order to understand the structural transformations that can occur in 2:17 type SmCo magnetic alloys containing Fe, Cu and Zr during various stages of heat-treatment, it is essential to understand the quinary Sm-Co-Fe-Cu-Zr phase diagram in the interested range of compositions. A complete description of quinary phase diagram for Sm-Co-Fe-Cu-Zr does not exist due to non-availability of sufficient experimental data. Moreover, under isobaric and isothermal conditions, the system exhibits four degrees of freedom and the usual representation of quinary phase diagram becomes complex. However, a pseudo binary phase diagram as a function of Sm concentration in Co at constant Fe, Cu and Zr has been reported by Morita *et al.* [9] and the experimental results on structural transformations in this study are explained based on this pseudo-binary diagram.

It can be seen from the phase diagram (Fig. 1) that the 2:17 phase exists in two different crystal structure types, viz. (i) hexagonal  $\text{Th}_2\text{Ni}_{17}$  (2:17 H) type at temperatures above 1273 K (at  $\text{Sm} \leq 10.5$  at%) and (ii) rhombohedral  $\text{Th}_2\text{Zn}_{17}$  (2:17 R) type at temperatures below 1273 K. In addition, there exists an hexagonal  $\text{TbCu}_7$  (1:7 H) type structure at temperatures above 1273 K (at  $\text{Sm} \geq 10.5$  at %). All these structures are modifications of the structure of  $\text{CaCu}_5$  type [12] and can be distinguished from the XRD patterns shown in Fig. 2 [9].  $\text{Th}_2\text{Zn}_{17}$  and  $\text{Th}_2\text{Ni}_{17}$  type structures are identified with the presence of (204) and (203) peaks (Fig. 2a and b) respectively. These reflections will be absent in the case of  $\text{TbCu}_7$  type structure.

#### 3.2. Investigations on as-cast alloy

Fig. 3 shows the optical micrograph of as-cast alloy A. It can be seen that the cast structure of the alloy consists of three phases: 2:17 matrix phase, a Sm-rich boundary phase and a Zr-rich needle like phase embedded in the boundary phase. Similar microstructural features have also been observed for the other two alloys. The chemical homogeneity of the cast alloys has been ensured through wet chemical analysis and SEM-EDS at various regions of the ingot. The average grain size of 2:17 matrix phase in the cast alloy is about  $200 \mu\text{m}$ , suggesting that the 2:17 particles, of size  $5\text{--}10 \mu\text{m}$ , are nearly single crystals. Therefore, a strong easy axis (*c*-axis)

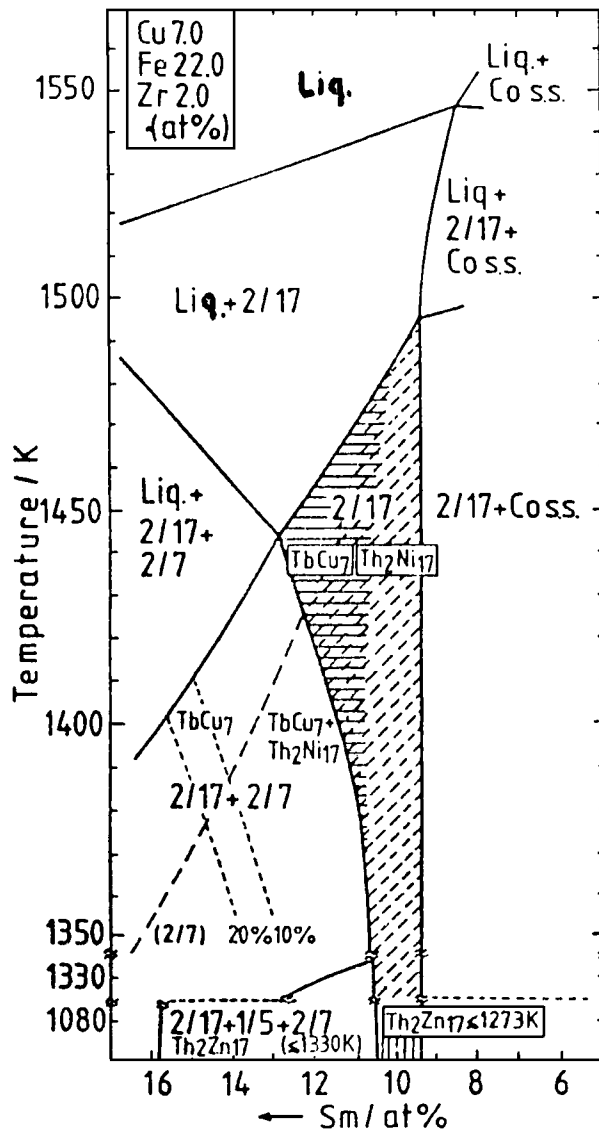


Figure 1 Vertical section of the quinary Sm-Co-Fe-Cu-Zr phase diagram [9].

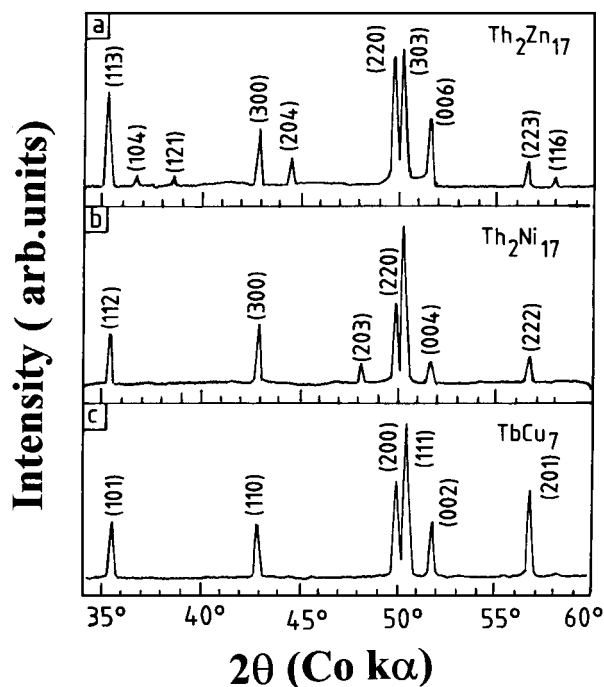


Figure 2 XRD patterns of 2:17 phase with three different structure types, viz.  $\text{Th}_2\text{Zn}_{17}$ ,  $\text{Th}_2\text{Ni}_{17}$  and  $\text{TbCu}_7$  [9].

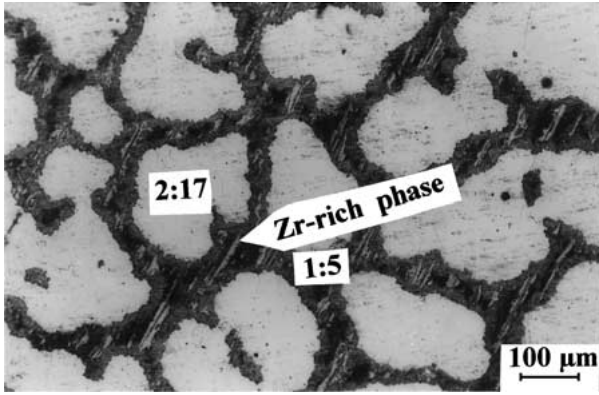


Figure 3 As-cast structure of alloy A showing three phase microstructure (2:17 as matrix, Sm-rich 1:5 type as boundary phase and Zr-rich needle like phase embedded in 1:5 phase).

of orientation is anticipated in the samples compacted under magnetic field. To investigate this, XRD studies were carried out on two samples of alloy A compacted with and without aligning magnetic field and the results are shown in Fig. 4. Considering the intensity of (001) peak of 2:17 phase as a measure of *c*-axis orientation of the particles, it can be seen from Fig. 4 that the samples compacted in magnetic field exhibits more magnetic anisotropy than those compacted without field.

### 3.3. Structural transformations

Fig. 5 shows X-ray powder diffraction patterns of alloy A quenched from solution treatment temperature of 1448 K (Fig. 5a) and after isothermal aging at 1108 K (Fig. 5b). It can be seen that the sample after solution treatment has a mixture of 1:7 H and partially transformed 2:17 R structures. After isothermal aging, the structure transforms fully into 2:17 R. Formation of 1:5 H phase in small volume fraction (6–8%) has also been seen in isothermally aged samples. A similar observation was also noticed in samples of alloy B. In the case of alloy C where Sm composition is <10.5 at%, the samples after solution treatment showed 2:17 H type structure (Fig. 6) and subsequent isothermal aging

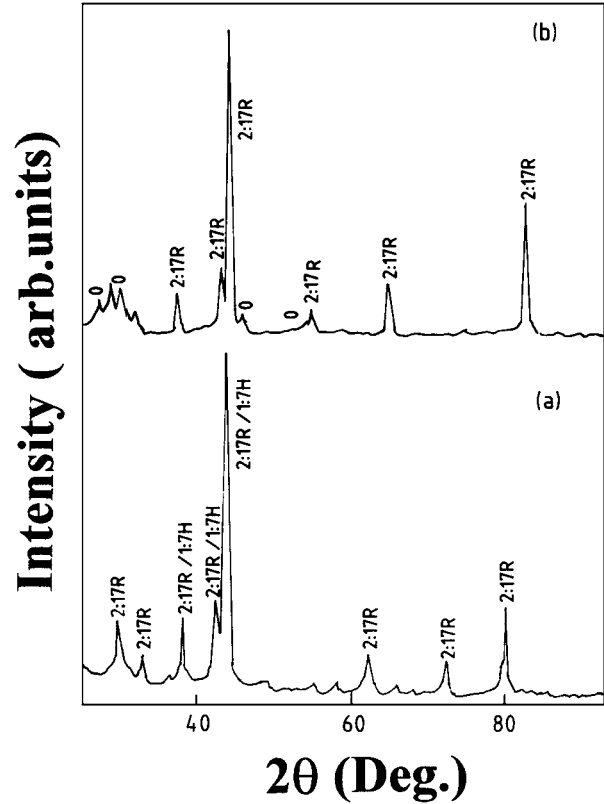


Figure 5 XRD patterns of alloy A. (a) Sintered at 1463 K and solution heat-treated at 1448 K. XRD pattern reveals that the sample after solution treatment has a mixture of  $TbCu_7 + Th_2Zn_{17}$  type structures. (b) Isothermally aged at 1123 K followed by slow cooling to 673 K. After isothermal aging the crystal structure of 2:17 phase transforms completely into  $Th_2Zn_{17}$  type (2:17 R) structure with precipitation of 1:5 type phase (marked as circles).

has not resulted in the necessary structural transformation. Hence this alloy was not investigated further in detail. These structural transformations can be understood through the pseudo binary phase diagram illustrated in Fig. 1. As seen from Fig. 1, the 2:17 single phase region exists in the Sm content ranging from 9.5 at% to 13 at% at high temperatures above 1100 K. The 2:17 phase exhibits at high temperature either the 2:17 H structure or

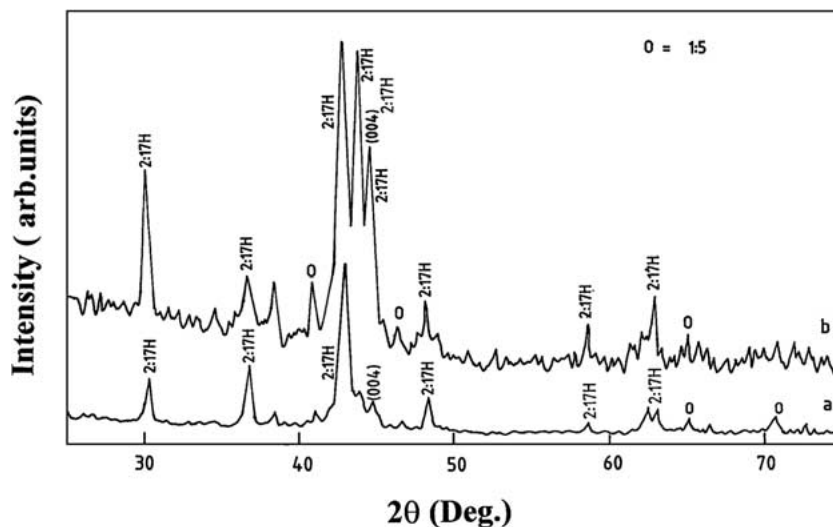


Figure 4 XRD patterns of green compact of alloy A. (a) without magnetic field alignment and (b) with magnetic field alignment. It can be seen that intensity of (004) peak of 2:17 H phase is relatively high suggesting particle orientation during magnetic field alignment.

TABLE II Structural transformations on thermal processing of 2:17 SmCo alloys

Processing	Structural transformations
Sintering (1463–1483 K)	2:17 H (Th <sub>2</sub> Ni <sub>17</sub> )
Solution treatment (1433–1463 K)	(i) 1:7 H (TbCu <sub>7</sub> ) or [1:7 H (TbCu <sub>7</sub> ) + partially transformed 2:17 R (Th <sub>2</sub> Zn <sub>17</sub> )] for 10.5 at% ≤ Sm ≤ 13.0 at% (ii) 2:17 H (Th <sub>2</sub> Ni <sub>17</sub> ) or [2:17 H (Th <sub>2</sub> Ni <sub>17</sub> ) + partially transformed 2:17 R (Th <sub>2</sub> Zn <sub>17</sub> )] for 9.5 at% ≤ Sm ≤ 10.5 at%
Isothermal aging (1073–1173 K)	(i) 2:17 R (Th <sub>2</sub> Zn <sub>17</sub> ) + 1:5 H (CaCu <sub>5</sub> ) + 1:7 H (TbCu <sub>7</sub> ) for 10.5 at% ≤ Sm ≤ 13.0 at% (ii) 2:17 R (Th <sub>2</sub> Zn <sub>17</sub> ) + untransformed 2:17 H (Th <sub>2</sub> Ni <sub>17</sub> ) for 9.5 at% ≤ Sm ≤ 10.5 at%

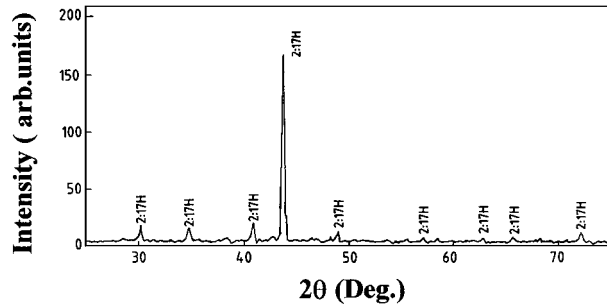


Figure 6 XRD pattern of alloy C after solution heat—treated at 1448 K showing Th<sub>2</sub>Ni<sub>17</sub> type structure of 2:17 phase.

the 1:7 H structure based on the Sm content, with latter forming at higher Sm content. On quenching from the solution treatment temperature, the 2:17 phase transforms from 2:17 H to disordered 1:7 H or [1:7 H + partially transformed 2:17 R] structure depending on the cooling rate. Subsequent isothermal aging at 1108 K will result in the transformation of completely ordered 2:17 R structure and is also accompanied by a precipitation of small volume fraction of 1:5 type phase [6]. The various structural transformations at different stages of thermal processing for the 2:17 phase are given in Table II.

### 3.4. Effect of isothermal aging

Samples from alloys A and B were subjected to different isothermal aging time and temperature and the effect on magnetic properties was studied in detail. Fig. 7a and b shows the dependence of magnetic properties [intrinsic coercivity (iHc), normal coercivity (Hc) and energy product ((BH)max.)] on isothermal aging time and temperature for alloys A and B respectively. It can be seen that the magnetic properties show a maximum at 1108–1123 K for a soaking time of 10–12 h. Fig. 8a–e shows the XRD patterns revealing the effect of isothermal aging temperature on phase formation in fully processed samples of alloy B. The peaks corresponding to 1:5 type phase are marked and this phase has been found to decrease initially with increasing temperature and then increases beyond 1123 K. It is observed that 1108–1123 K is optimal for an isothermal aging time of 10–12 h corroborating the results shown in Fig. 8. The samples exhibited an energy product of 152 kJ/m<sup>3</sup> with

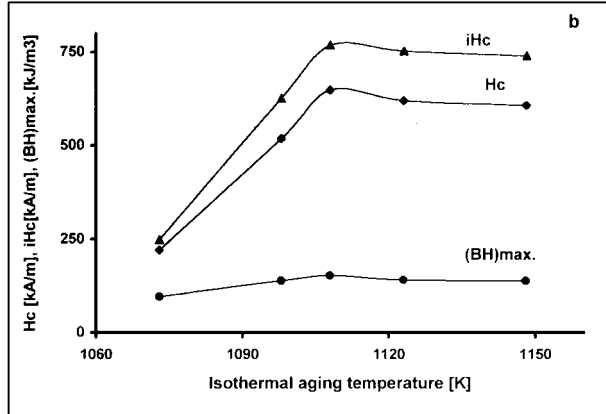
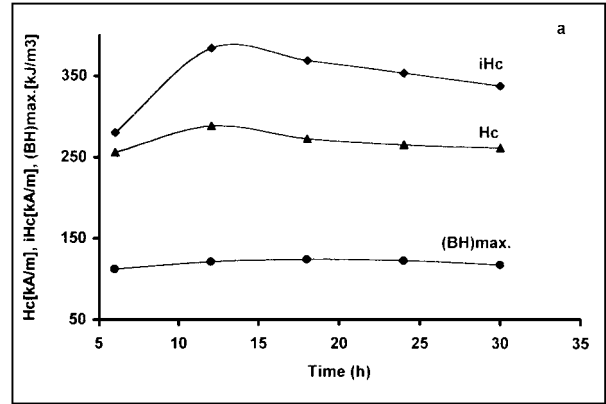


Figure 7 Effect of isothermal aging time and temperature on magnetic properties. (a) for alloy A and (b) for alloy B. The properties are maximum at 1108–1123 K for 10–12 h of aging time.

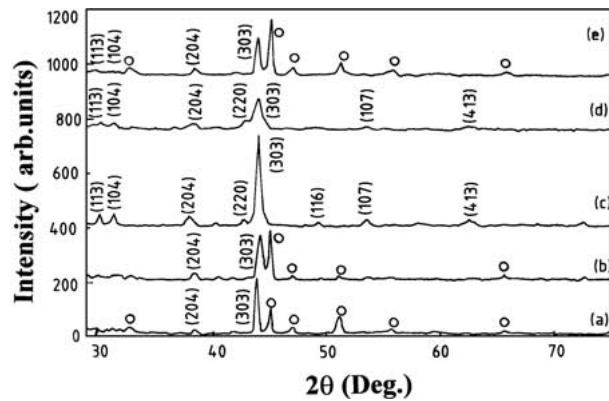


Figure 8 XRD patterns showing the effect of isothermal aging temperature (aging time 10–12 h) on phase formation for alloy A. The peaks marked as ‘o’ correspond to 1:5 type phase. This phase decreases initially with increasing of temperature and then increases beyond 1123 K. Thus 1108–1123 K is found to be optimal for isothermal aging corroborating the results shown in Fig. 7.

an intrinsic coercivity of 450 kA/m. The degradation of magnetic properties with increase in isothermal aging temperature and time may be due to increase in volume fraction of the 1:5 type phase and the associated decrease in domain wall energy difference between 2:17 and 1:5 phases [13].

### 3.5. Microstructural characterization

#### 3.5.1. Optical and SEM

Fig. 9 shows the optical microstructure of the sample of alloy A after isothermal aging at 1108 K for

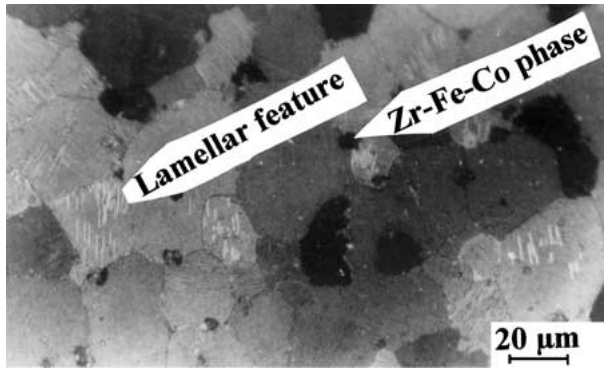


Figure 9 Optical microstructure of alloy A after isothermal aging at 1108 K. Lamellar feature is seen in a few grains of 2:17 R phase. Zr-Fe-Co rich phase is also present in the alloy.

10 h. Lamellar feature has been seen in a few grains of 2:17 matrix. The secondary phases such as  $\text{Sm}_2\text{O}_3$  and Zr-Fe-Co rich phase present in the samples have been identified by SEM elemental mapping (Fig. 10). Zr-Fe-Co rich phase is a soft magnetic phase and its composition (in at%) is estimated as 23Zr-17Fe-60Co [ $\text{Zr}_6(\text{FeCo})_{23}$ ] through SEM-EDS. Presence of this phase is detrimental to realize high coercivity in 2:17 magnets [3].

### 3.5.2. TEM studies

Detailed TEM studies have been carried out on isothermally aged samples of alloy A for analysing the structure type and coherency between the phases. Fig. 11 a–d

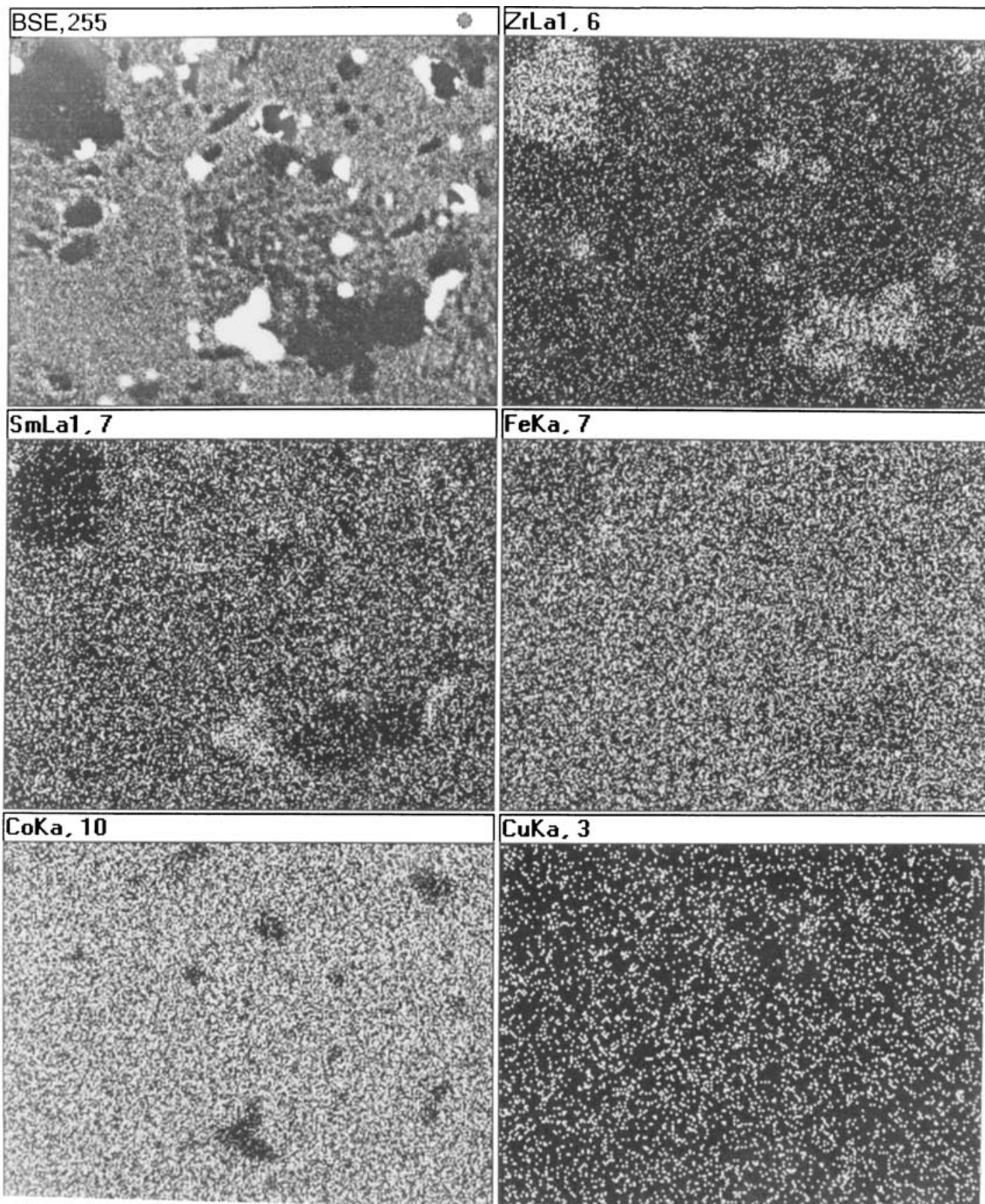


Figure 10 SEM back-scattered image of alloy A after isothermal aging at 1108 K. From elemental mapping the presence of Zr-Fe-Co rich phase has been identified. Through EDS analysis the composition of the phase is found to be  $\text{Zr}_6(\text{FeCo})_{23}$ .

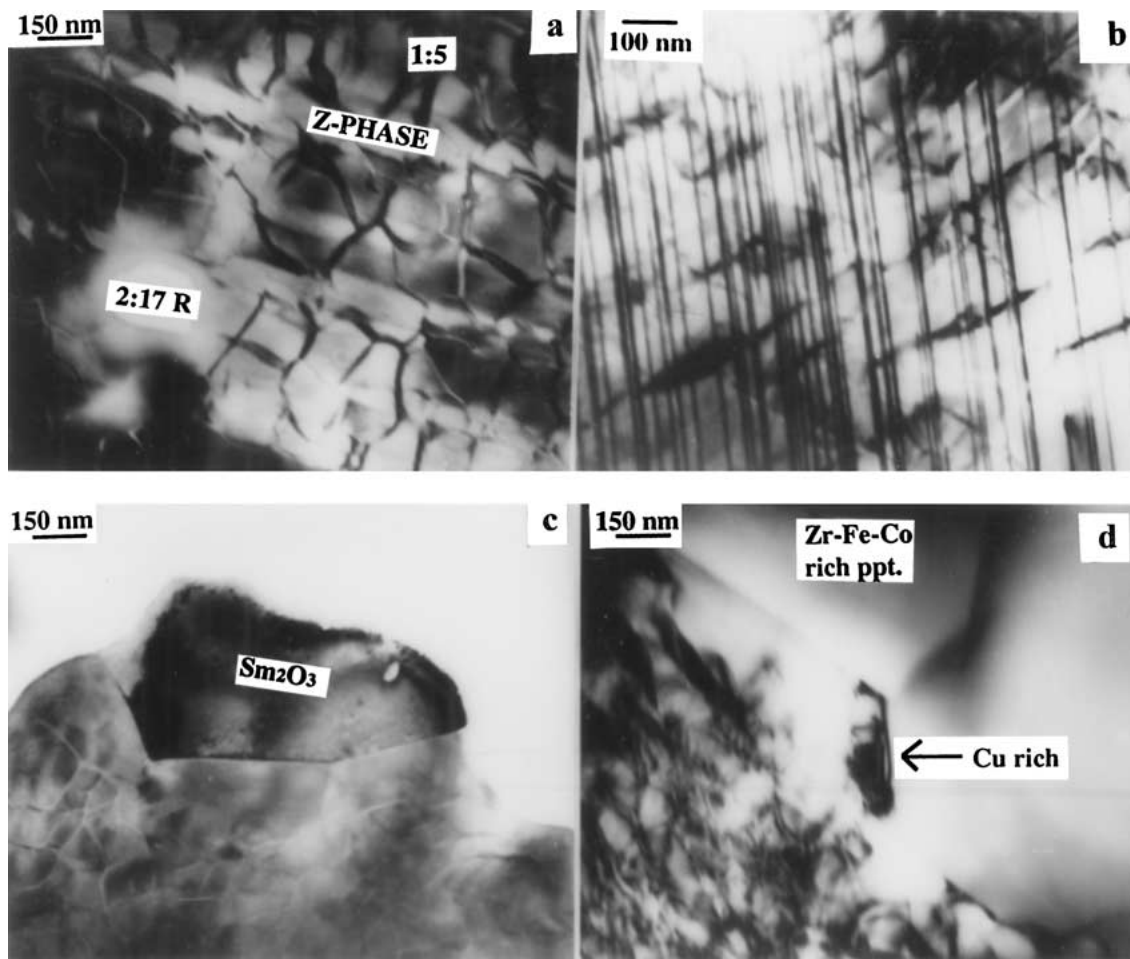


Figure 11 TEM micrographs of alloy A after isothermal aging at 1108 K followed by slow cooling to 673 K. (a) Cellular precipitate microstructure with cells as 2:17 R and cell boundaries as 1:5 type phase. Cell size is 150–200 nm. (b) Dark field image showing thin platelets of Zr-rich phase running across many cells and cell boundaries. (c and d) Presence of secondary phases such as Zr-Fe-Co,  $\text{Sm}_2\text{O}_3$  and a Cu-rich precipitate.

shows TEM micrographs of sample of alloy A. It can be seen from Fig. 11a that the sample exhibits cellular precipitate microstructure and this observation is consistent with many authors [3–5]. Electron diffraction studies have shown cell interiors as 2:17 R phase and the cell boundary as 1:5 H type phase. The cell size was estimated to be of the order of 200 nm. TEM-EDS studies showed that the cell interior was poorer in Zr, Cu and cell boundary was richer in Cu. In addition to cellular precipitates, Zr-rich long platelets were also seen running across many cells and cell boundaries. Fig. 11b is the dark field image of the platelet phase in an edge on orientation such that (0001) planes of the phase is parallel to the electron beam. The thickness of the platelet phase has been estimated to be < 1 nm.

With respect to crystal structure of the platelet phase, two different types have been reported, viz. (i) 1:3 H type structure by Rabenberg *et al.* [4] and Hadjipanayis *et al.* [3] and (ii) 2:17 H type structure by Fidler *et al.* [14]. On the other hand, from the selected area diffraction pattern obtained from the platelet phase (Fig. 12), the present studies reveal that the platelet phase is of 1:7 H type structure. The mechanism of formation of platelet phase with 1:7 H structure may be explained based on two possibilities: (i) the platelet phase is a retained form of the high temperature 1:7 H phase or (ii) the high temperature phase of 2:17 H type is retained

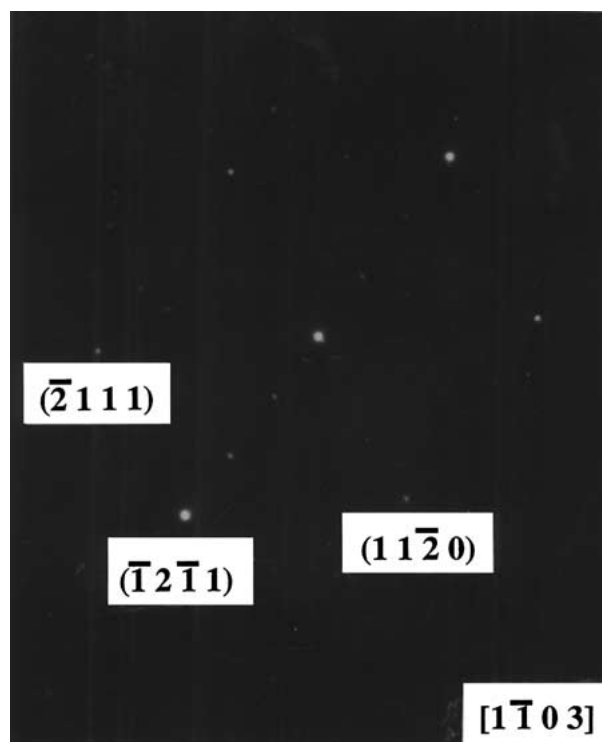


Figure 12 Electron diffraction pattern of Zr-rich platelet phase. Simulation of electron diffraction pattern showed that the phase is of  $\text{TbCu}_7$  type structure.

as disordered 1:7 H type phase on solution treatment. On isothermal aging the disordered 1:7 H phase transforms to an ordered 2:17 R phase with simultaneous precipitation of 1:5 type boundary phase and in addition, the partly retained 1:7 H phase which is richer in Zr comes out as platelet phase. However, detailed TEM studies are required on solution treated samples to confirm the above possibilities. Such studies are underway and the results will be reported elsewhere [15].

TEM investigations also revealed the presence of  $\text{Sm}_2\text{O}_3$  particles, Zr-Fe-Co rich phase and a Cu-rich phase (Fig. 11c and d) and the presence of these phases in the final microstructure would reduce the magnetic properties. The effect of Zr on the formation of the Zr-Fe-Co rich phase and magnetic properties is another interesting area and further studies in this direction are also under progress.

#### 4. Conclusion

From the microstructural and magnetic characterization studies on three different compositions of 2:17 type quinary Sm-Co alloys, the following conclusions are drawn:

(i) Sm-rich compositions ( $> 10.5$  at%) produce single phase  $\text{TbCu}_7$  type structure after solution treatment. For Sm-poor compositions ( $< 10.5$  at%), the crystal structure is found to be  $\text{Th}_2\text{Ni}_{17}$  type.

(ii) Effect of time and temperature for isothermal aging on magnetic properties revealed that temperature in the narrow range of 1108–1123 K for a soaking time of 10 h is optimal for magnetic properties.

(iii) TEM studies show cellular precipitate microstructure with cells as 2:17 R and the boundary phase as 1:5 type structures. Zr-rich platelets are also seen running across many cells and cell boundaries and electron diffraction studies reveal that this phase is of 1:7 H type structure.

#### Acknowledgments

The authors are grateful to Vikram Sarabhai Space Centre, Trivandrum for the financial support to carry out this work. The keen interest shown by Defence Research and Development Organisation, Government of India in this work is also gratefully acknowledged.

#### References

1. T. OJIMA, S. TOMIJAWA, T. YONEYAMA and T. HORI, *IEEE Trans. Magn.* **MAG-13** (1977) 1317.
2. S. LIU and A. E. RAY, *ibid.* **MAG-25** (1989) 3785.
3. G. C. HADJIPANAYIS, E. J. YADLOUSKY and S. H. WOLLINS, *J. Appl. Phys.* **53** (1982) 2386.
4. L. RABENBERG, R. K. MISHRA and G. THOMAS, *ibid.* **53** (1982) 2389.
5. B. Y. WONG, M. WILLARD and D. E. LAUGHLIN, *J. Magn. Magn. Mater.* **169** (1997) 178.
6. A. E. RAY, *IEEE Trans. Magn.* **MAG-20** (1984) 1614.
7. Y. MORITA, T. UMEDA and Y. KIMURA, *ibid.* **MAG-23** (1987) 2702.
8. M. Q. HUANG, W. E. WALLACE, M. E. MCHENRY, Q. CHEN and B. M. MA, *J. Appl. Phys.* **83** (1998) 6718.
9. Y. MORITA, T. UMEDA and Y. KIMURA, in Proc. of the MRS Int. Meeting on Advanced Materials, edited by M. Doyama, S. Somya and R. P. H. Chang, May-31–June 3, 1988, Sunshine City, Ikebukura, Tokyo, Japan, Vol. 11, p. 97
10. H. SAITO, M. TAKAHASHI, T. WAKIYAMA, G. KODONAD and H. NAKAGAWA, *J. Magn. Magn. Mater.* **82** (1989) 322.
11. A. J. PERRY and A. MENTH, *IEEE Trans. Magn.* **MAG-11** (1975) 1423.
12. W. GONG, B. M. MA and C. O. BOUNDS, *J. Appl. Phys.* **83** (1998) 6709.
13. J. D. LIVINGSTON and D. L. MARTIN, *ibid.* **48** (1977) 1350.
14. J. FIDLER, P. SKALICKY and F. ROTHWARF, *IEEE Trans. Magn.* **MAG-19** (1983) 2041.
15. K. MURALEEDHARAN, R. GOPALAN, T. S. R. K. SASTRY, D. V. SRIDHARA RAO and V. CHANDRA-SEKARAN, unpublished work.

Received 21 August 2000

and accepted 19 April 2001